MedChemComm

REVIEW

View Article Online
View Journal | View Issue

Cite this: *Med. Chem. Commun.*, 2019, **10**, 1569

Molecular evolution of peptides by yeast surface display technology†

Sara Linciano, ‡[a] Stefano Pluda, ‡[ab] Arianna Bacchin [a] and Alessandro Angelini *[ac]

Received 29th April 2019,
Accepted 28th June 2019

DOI: 10.1039/c9md00252a

rsc.li/medchemcomm

Genetically encoded peptides possess unique properties, such as a small molecular weight and ease of synthesis and modification, that make them suitable to a large variety of applications. However, despite these favorable qualities, naturally occurring peptides are often limited by intrinsic weak binding affinities, poor selectivity and low stability that ultimately restrain their final use. To overcome these limitations, a large variety of *in vitro* display methodologies have been developed over the past few decades to evolve genetically encoded peptide molecules with superior properties. Phage display, mRNA display, ribosome display, bacteria display, and yeast display are among the most commonly used methods to engineer peptides. While most of these *in vitro* methodologies have already been described in detail elsewhere, this review describes solely the yeast surface display technology and its valuable use for the evolution of a wide range of peptide formats.

1. Introduction

Genetically encoded peptides are being increasingly utilized in diverse therapeutic, diagnostic and biotechnological applications.[1] They possess distinctive properties including a small size (2–50 amino acids long), access to chemical synthesis, ease of modification, low toxicity and reduced antigenicity. However, despite these favorable qualities, naturally occurring peptides often exhibit weak affinities, poor selectivity and low stability. To overcome these limitations, a large variety of strategies have been developed over the past few decades to engineer peptide molecules with desired enhanced properties. Some of these approaches are inspired by chemical modifications occurring on non-ribosomal peptides[2] such as the incorporation of non-proteinogenic amino acids, modifications of the peptide backbone and cyclization.[3]

Alternatively, genetically encoded peptide ligands with tailored properties have been generated by screening large combinatorial libraries using *in vitro* display techniques.[4,5] Phage display was the first technique developed and is still the most commonly used method to engineer peptides.[6] Since then, different biological selection methods have been established and rapidly developed for the directed evolution of peptides. The most widely used are mRNA display,[7] ribosome display,[8] bacteria display[9] and yeast display.[10] All these techniques rely on a physical linkage between the displayed peptide ('phenotype') and its encoding DNA or RNA sequence ('genotype'). By using such technologies peptide ligands with desired properties are evolved according to Darwinian principles including diversification, selection and amplification. While most of these strategies have been thoroughly described elsewhere,[11–13] this review focuses exclusively on genetically encoded peptides that have been evolved by using yeast surface display technology.

2. Yeast surface display technology

Since its invention in 1997, yeast surface display has become a popular tool for protein engineering and library screening applications.[10] The technique was first validated to enhance the affinity of existing proteins, but subsequently proved its effectiveness for isolating *de novo* molecules from naive combinatorial libraries of multiple immunoglobulin and non-immunoglobulin scaffolds, including some peptides.[14–16] In addition to tuning the affinity and specificity of multiple proteins and peptides towards a wide range of targets, yeast surface display technology has also been successfully used for epitope mapping, to improve the recombinant production and the stability of the molecules of interest as well as to engineer the function of several enzymes.[14–16]

Although diverse yeast strains and various cell wall anchors have been used to display a large variety of protein and peptide scaffolds,[17–19] the *Saccharomyces cerevisiae* Aga1–Aga2 display system remains the most commonly used. In

[a] *Department of Molecular Sciences and Nanosystems, Ca' Foscari University of Venice, Via Torino 155, Venezia Mestre 30172, Italy*
[b] *Fidia Farmaceutici S.p.A, Via Ponte della Fabbrica 3/A, Abano Terme 35031, Italy*
[c] *European Centre for Living Technology (ECLT), Ca' Bottacin, Dorsoduro 3911, Calle Crosera, Venice 30123, Italy. E-mail: alessandro.angelini@unive.it*

† Electronic supplementary information (ESI) available. See DOI: 10.1039/c9md00252a

‡ The authors contributed equally to this work.

this arrangement, the molecule of interest is expressed as fusion to the Aga2 protein that is linked to the membrane anchored a-agglutinin Aga1 protein through two disulfide bridges, resulting in a covalent complex on the surface of the yeast cell. Proteins and peptides of interest can be displayed on the yeast surface as either C- or N-terminal fusions to the Aga2 protein (Fig. 1a and b).[14,16] Recently, Cochran and colleagues have developed a novel dual Aga1–Aga2 yeast display strategy that appear to simplify quantification of binding interactions on the yeast cell surface (Fig. 1c).[18] Each yeast cell displays approximately 10^4–10^5 copies of the Aga2 fusion on its surface, although individual expression levels may vary depending on the stability and solubility of the displayed molecule. Moreover, alternative methods based on a "secretion-and-capture" approach have been successfully applied.[20,21] Finally, efficacious yeast-based "switchable" display/secretion systems exploiting amber codon suppression[22] and ribosomal skipping[23] have also been recently reported.

Yeast surface display technology offers several advantages over other display systems. First, it relies on an eukaryotic expression machinery capable of incorporating post-translational modifications (*e.g.* disulfide isomerization) enabling the folding and secretion of difficult proteins and peptides that may be otherwise refractory to other *in vitro* display systems.[14,16] Second, and probably the greatest advantage of yeast display compared to other *in vitro* display technologies, is its compatibility with fluorescence-activated cell sorting (FACS) that allows high-throughput screening and biophysical characterization of large combinatorial libraries of proteins and peptides (Fig. 1d).[14,16]

The majority of yeast surface display constructs generally include two epitope tags at the N- and at the C-terminus of the molecule of interest fused to Aga2. These epitope tags allow quantification of the full-length fusion expression and normalization of function to surface expression by flow cytometry. Similarly, binding to the target of interest can be determined by incubating yeast cells with the labeled target. By using a two-color labeling scheme, with one fluorescent probe for expression and another for target binding, proteins and peptides of interest can be engineered for affinity, specificity and stability concomitantly.[14,16] Flow cytometry can also be used for the biophysical and quantitative characterization of individual variants as cell-surface fusions without the need for sub-cloning, soluble expression and purification.[14,16] By applying different labeling approaches, including equilibrium binding and kinetic competition, yeast display combined with flow cytometry allows quantitative and fine discrimination between variants with different binding affinities for the target.[24] By normalizing the median fluorescence intensity from the binding signal to the median fluorescence intensity from the display signal, as a function of protein concentration, is possible to determine the equilibrium dissociation constant (K_d) of each individual selected clone. Importantly, previous studies have demonstrated that the K_d values determined using yeast surface display are in agreement with those measured using alternative techniques such as fluorescence polarization, surface plasmon resonance and biolayer interferometry.[14,16]

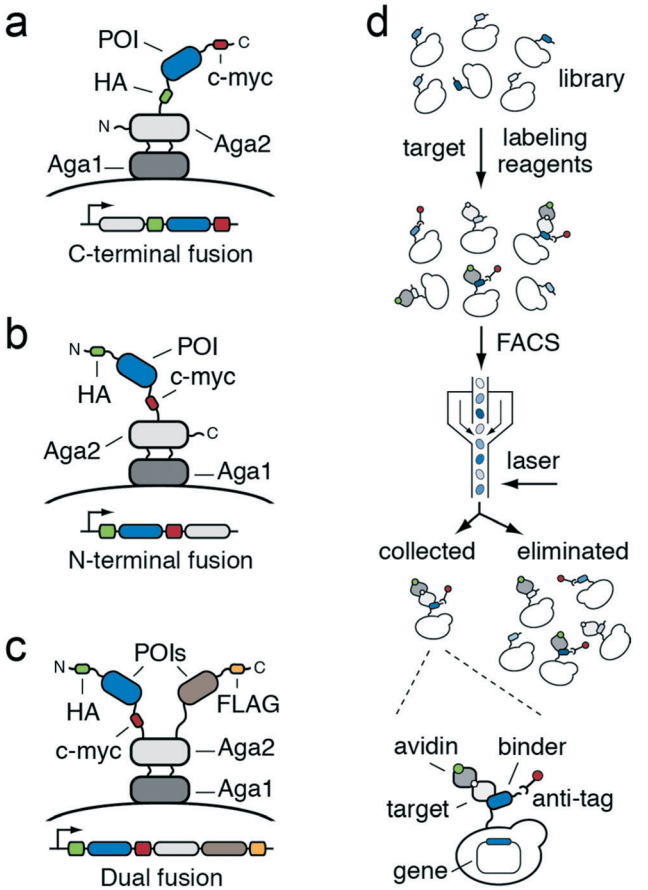

Fig. 1 Schematic representation of the yeast display technology based on Aga1–Aga2 system. a) The protein or peptide of interest (POI, *blue*) is displayed as a C-terminal fusion to the Aga2 protein (*light grey*), flanked by two tags for immunofluorescent detection: the hemagglutinin (HA) epitope tag at the N-terminus (*green*) and the c-myc epitope tag at the C-terminus (*red*). The Aga2 protein forms two disulfide bonds with the membrane-anchored Aga1 protein (*dark grey*); b) the POI (*blue*) is displayed as a N-terminal fusion to the Aga2 protein (*light grey*), flanked by the HA tag at the N-terminus (*green*) and the c-myc tag at the C-terminus (*red*); c) co-expression of two different POIs (*blue* and *brown*) fused at the N- and at the C-terminus of the Aga2 protein (*light gray*). The first POI (*blue*) is flanked by the HA tag (*green*) at the N-terminus and the c-myc tag at the C-terminus (*red*) whereas the second POI (*brown*) has a FLAG tag (*orange*) at the C-terminus; d) schematic representation for the selection of engineered POIs from a yeast display library by using fluorescence-activated cell sorting (FACS). Yeast cells, each displaying a different POI variant (*light to dark blue*), are incubated with a biotinylated target (*light gray with white dot*). Addition of fluorescently-labeled affinity reagents against the c-myc epitope (*red*) and the biotin (*dark grey with green dot*) enables the selection of dual positive yeast clones displaying full-length and properly folded POI that bind to the soluble target of interest. The FACS and two-color labeling allow the binding affinity to be normalized to cell surface expression and the affinities between clones accurately discriminated.

However, the yeast display technology is not without its limitations. First, the library size diversity (~10^7–10^9) is usually a few orders of magnitude lower than that obtained with

other systems. Second, the presence of multiple copies of a displayed protein or peptide on the surface of yeast could lead to undesired polyvalent interactions that synergize to enhance the apparent binding affinity.[25] This effect is commonly referred to as 'avidity' and can occur only when the soluble target is multivalent, and its binding sites are sufficiently close together to be simultaneously recognized by multiple copies of proteins or peptides present on the surface of yeast. Such polyvalent interactions lead to increases in the residence time and in the local concentration of the target thus favoring its binding and rebinding and ultimately resulting in often undesired higher binding affinities.[25] Third, the technique is still hampered by the low flow rate ($\sim 10^7$ cells per hour) of the majority of flow cytometry instruments currently available. However, while these drawbacks are crucial for large proteins, they are in general less critical for short peptides for which the diversity to be covered is smaller and the high avidity beneficial when working with weak peptide binders or substrates otherwise undetectable. Moreover, if necessary, multivalent binding can be overcome by applying kinetic strategies in the presence of large amounts of a competitive target able to interfere in a concentration-dependent manner.[14,16] Using such approach, the yeast cells displaying the protein or peptide of interest are initially incubated with the labeled target and the unbound fraction removed by washing. The labeled cells are following incubated with a large excess of unlabeled target to prevent rebinding of the labeled one after dissociation. Hence, protein or peptide variants displayed on the surface of yeast cells can be discriminated based on their dissociations rate constants (k_{off}) with variants having the higher affinity retaining the largest percentage of initially bound labeled target.[14,16] Considering all these factors, yeast display represents a versatile and suitable tool for the design and engineering of a wide variety of peptides.

3. Genetically encoded peptides displayed on yeast

Over the last fifteen-years, yeast display has been used to engineer an increasing number of genetically encoded linear, cyclic and well-structured peptides. These peptides and their applications are discussed in the following sections.

3.1. Linear peptides

Protein–protein interactions are essential for almost all intracellular and extracellular biological processes and play a critical role in various diseases and pathological conditions.[3] A considerable portion (15–40%) of these interactions is mediated by short linear peptide motifs.[26] There is therefore great interest in modifying these naturally occurring sequences in order to understand their binding properties and develop novel molecules with enhanced features.[3,27]

A well-known example of linear peptides involved in transient protein–protein interactions comes from the Bcl-2 family of proteins. In human this family comprises five pro-survival members (Bcl-2, Mcl-1, Bfl-1, Bcl-x_L, and Bcl-w) that interact with proapoptotic proteins comprising a ~23-residue Bcl-2-homology-3 (BH3) motif.[28] This peptide sequence is intrinsically disordered but forms an α-helix upon binding to the target. Importantly, overexpression of Bcl-2 proteins has been shown to contribute to cancer progression and chemotherapy resistance.[29] While an encouraging antitumor activity has been observed with some compounds, their therapeutic utility was often limited by toxicities associated to the interaction with multiple members of the family. As a result, there is a great interest in developing Bcl-2 inhibitors with anti-apoptotic function that can selectively target a single Bcl-2 member.[30] Toward this goal, Keating and colleagues integrated the strengths of yeast display and computational modelling to map the affinities and the specificities of thousands of BH3 peptides in parallel (Fig. 2a). In a pioneer study, Dutta *et al.* applied yeast surface display technology to screen a randomized library of the BH3 motif of Bim and identified variants capable of binding with sub-nanomolar affinities and remarkable selectivity to either Mcl-1 or Bcl-x_L proteins (Tables 1 and S1†).[31] Similarly, highly specific BH3-like peptides were later isolated against other human pro-survival proteins (Tables 1 and S1†).[32–34] Recently, Reich *et al.* developed "Sortcery", an optimized high-throughput method to rank $>10^3$ BH3-like peptides displayed on yeast with respect to their affinities for an anti-apoptotic target.[35,36] An analogous strategy was used to re-engineer PUMA, a promiscuous binder of multiple anti-apoptotic proteins, to make it 150-fold more selective for Bfl-1 both as a non-covalent and as a covalent inhibitor, respectively (Tables 1 and S1†).[37] Finally, by applying an advanced version, named "Amped Sortcery", Jenson *et al.* succeeded in determining the binding affinities and selectivity of a larger library ($\sim 10^4$) of computational designed BH3-like peptides toward three Bcl-2 family proteins: Bcl-x_L, Mcl-1 and Bfl-1 (Fig. 2b).[38] The data generated were used to build a model of the peptide-binding landscape that assisted the identification of novel peptides capable of binding with high affinity (K_d = 0.6–3.7 nM) and at least 300-fold improved specificity to just one member of the family (Tables 1 and S1†).[38] These peptides constitute promising starting leads for the development of therapeutics directly targeting the Bcl-2 family proteins. Their chemical modification by hydrocarbon stapling has already proven effective for developing enhanced and cell-permeable peptide inhibitors.[39–41]

Another example of important transient protein–protein interaction in which linear peptides play a key role is represented by the binding of T-cell receptors (TCR) to the antigenic peptides loaded on the major histocompatibility complex (MHC) classes I and II.[42] The MHC class I molecules are expressed by all nucleated cells and can accommodate antigenic peptides of 8–10 amino acids in length whereas the MHC class II molecules are primarily expressed by professional antigen-presenting cells (APCs) and can lodge peptides with greater length (13–24 amino acids) thus allowing

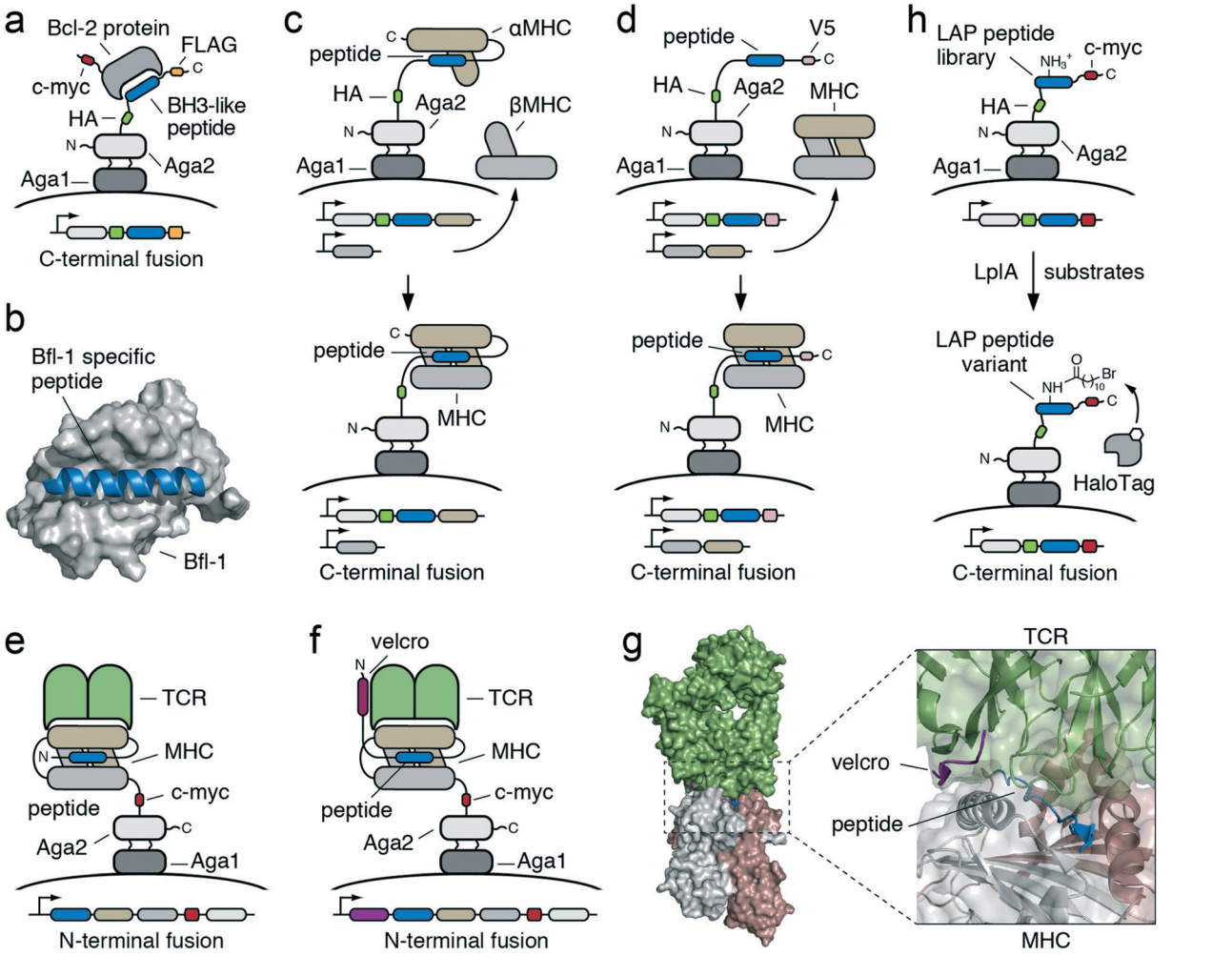

Fig. 2 Schematic representation of linear peptides evolved using yeast display technology. a) BH3-like peptides (*blue*) are displayed on the surface of yeast as a C-terminus fusion of the Aga2 protein (*light gray*) and recognized by a Bcl-2 protein (*dark gray*); b) crystal structure of human Bfl-1 (*gray surface*) in complex with a Bfl-1-specific peptide (*blue cartoon*, PDB code: 6E3I); c) *Top*, the peptide (*blue*) located at the N-terminus of the αMHC subunit (*brown*), is displayed on the surface of yeast as a C-terminus fusion of the Aga2 protein (*light gray*) while the βMHC subunit (*medium gray*) is produced and secreted in a soluble form. *Bottom*, interaction between the displayed Aga2–peptide–αMHC fusion and the secreted βMHC leads to the assembly of a functional peptide-loaded MHC complex on the surface of yeast; d) *Top*, the peptide (*blue*), fused to the C-terminus of the Aga2 protein (*light gray*), is displayed on the surface of yeast while the whole dimeric MHC (*brown* and *medium gray*) is secreted in a soluble form. *Bottom*, formation of the peptide-loaded MHC complex on the surface of yeast is driven by non-covalent interactions between the displayed peptide and the secreted MHC molecule; e) the loaded peptide (*blue*), linked to the whole dimeric MHC (*brown* and *medium gray*), is encoded as a unique molecule and displayed on the surface of yeast as a N-terminus fusion of the Aga2 protein (*light gray*). Functional peptide-loaded MHC complex displayed on the surface of yeast is recognized by the soluble dimeric TCR receptor (*green*); f) an additional peptide sequence, named "velcro" (*purple*), is placed at the N-terminus of the loaded peptide (*blue*) and is displayed on the surface of yeast as a fusion of the whole dimeric MHC (*brown* and *medium gray*) and Aga2 (*light gray*) proteins; g) *Left*, crystal structure of a TCR (*green surface*) in complex with a peptide (*blue cartoon*) loaded on a MHC (*brown and medium gray surface*) in the presence of the affinity-enhancing "velcro" peptide (*purple*, PDB code: 6BGA). *Right*, close-up of the velcro-peptide–MHC–TCR complex; h) *Top*, LplA acceptor peptide (LAP, *blue*), fused to the C-terminus of Aga2 protein (*light gray*), is displayed on the surface of yeast and recognized by the LplA enzyme that catalyzes the conjugation of the 11-bromoundecanoic acid (*bottom*), an alkyl bromide that can be further specifically and covalently modified by the self-labeling enzyme HaloTag (*medium grey*). The white hexagon represents any probe. The epitope tags flaking the engineered peptides are colored in *green* (HA), *red* (c-myc), *orange* (FLAG) and *pink* (V5).

superior flexibility in peptide binding.[42,43] These interactions are central to many aspects of adaptive immunity including transplantation, infection, vaccination and autoimmunity. However, the very low affinity (K_d ~ 1–100 μM) and fast kinetics of TCR–peptide–MHC binding, along with the high conformational plasticity of TCR loops, consent a single TCR to recognize structurally distinct peptides presented by a common MHC molecule.[43,44] This peptide cross-reactivity hinders the development of TCRs as therapeutics because of its potential to induce off-target immune toxicity. Therefore, a deeper understanding of the TCR–peptide–MHC recognition would be of great value for the development of novel therapeutics with tailored antigen-binding specificities for the fine-tuning of the immune system. A way to explore and

Table 1 Linear peptides evolved using yeast display technology. Indicated dissociation constant (K_d), inhibition constant (K_i), half maximal effective concentration (EC_{50}), Michaelis–Menten constant (k_m) and catalytic constant (k_{cat}) values were reported as published. Legend: BH3 = Bcl-2-homology-3 motif; Bim = Bcl-2-like protein 11; Puma = Bcl-2-binding component 3; Mcl-1 = myeloid cell leukemia sequence 1; Bcl-x_L = B-cell lymphoma-extra large; Bfl-1 = Bcl-2-related protein A1; TCR = T-cell receptors; HLA = human leukocyte antigen; QL9 = peptide epitope of 2-oxogluterate dehydrogenase; MCC = moth cytochrome C; LplA = *Escherichia coli* lipoic acid ligase; LAP = LplA acceptor peptide; IL-2 = interleukin-2, CD69 = cluster of differentiation 69; * = specificity for single target molecule: # = only the values for the higher affinity peptides are reported

		Yeast display engineering		
Peptide	Target	Before	After	Ref.
Bim BH3	Mcl-1	K_i = 1.9 nM (<2-fold*)	K_i = 4 nM (>250-fold*)	31
	Bcl-x_L	K_i = 1.3 nM (<2-fold*)	K_i = 2.9 nM (>25-fold*)	
	Bfl-1	K_d = 4 nM (<4-fold*)	K_d < 0.3 nM (>27-fold*)	32
	Mcl-1	K_d = 0.8 nM (<18-fold*)	K_d = 1.9 nM (>680-fold*)	33
	Bcl-x_L	K_i < 0.1 nM (<2-fold*)	K_i = 0.09 nM (>180-fold*)	34
Puma BH3	Bfl-1	K_i = 2.4 nM (<2-fold*)	K_i = 15 nM (>150-fold*)	37
	Bfl-1	K_i = 4.8 nM (<0.5-fold*)	K_i = 3.2 nM (>300-fold*)	38
	Mcl-1	K_i = 1.69 nM (<2.8-fold*)	K_i = 0.6 nM (>6600-fold*)	
	Bcl-x_L	K_i = 1.00 nM (<4.8-fold*)	K_i = 3.7 nM (>1000-fold*)	
QL9	TCR-42F3	K_d = 399 μM	K_d = 3.4–9.7 μM# (>30-fold)	48
		K_d = 40 μM	K_d = 0.1–10 μM# (>4-fold)	50
		$EC_{50\text{-IL2}}$ = 0.0447 μM	$EC_{50\text{-IL2}}$ = 0.164 nM (>270-fold)	
HLA-B35	TCR55	K_d = 17 μM	K_d = 0.5–12.5 μM (1.5–34-fold)	49
		$EC_{50\text{-CD69}}$ >100 μM	$EC_{50\text{-CD69}}$ = 1.2–9.3 μM (>80-fold)	
Velcro-MCC	TCR2B4	K_d = 14.6 μM	K_d = 2.8 μM (~5-fold)	54
Velcro–Pep17		K_d = 159.6 μM	K_d = 15.4 μM (~10-fold)	
LAP2	LpIA	k_{cat}/k_m < 0.0135 μM^{-1} min^{-1}	k_{cat}/k_m = 0.99 μM^{-1} min^{-1} (>70-fold)	55

map the molecular properties of these interactions is by applying high-throughput *in vitro* display technologies. The heterodimeric nature of MHC molecules with intrachain disulfide bonds, an intrinsic low stability and lack of a native conformation in absence of bound antigen peptide, make the MHC not suitable for most of the traditional *in vitro* display techniques. To overcome these limitations, Boder *et al.* took advantage of the eukaryotic machinery of yeast and developed a system able to correctly assemble and display a functional wild-type peptide–MHC-II molecule (Fig. 2c).[45] Although the work did not involve any peptide engineering, the study paved the way to the use of yeast surface display for engineering and analyzing the properties of the TCR–peptide–MHC interaction. Few years later, Jang and Boder described an alternative system wherein peptide and MHC-II molecules are co-displayed on the surface of yeast in an intracellular association-dependent manner and their relative binding assessed by flow cytometry (Fig. 2d).[46] By using this system, the authors were able to quantitatively evaluate the binding of a specific MHC-II molecule to peptides mutated at a key anchor position and further evolve novel mutants with altered specificities. Yeast display technology combined to high-throughput FACS-based screening further led to the development of a novel system to identify CD4+ T-cell epitopes from antigens. By displaying a pathogen-derived peptide library of 10–20 amino acids fused to the single-chain MHC-II molecule on the surface of yeast, Wen *et al.* were able to identify a specific MHC-binding epitope from both the single HA protein and the entire influenza virus genome.[47] In the last ten years Garcia and colleagues have extensively implemented and applied yeast display technology to investigate the interrelationship between TCR–peptide–MHC binding and identified new peptide sequences reactive with a single TCR.[48–51] By screening randomized yeast-displayed peptide–MHC-I libraries, Adams *et al.* isolated a large collection of 9-amino acid peptides that bind a given TCR with affinities in the 3.4 to 9.7 μM range (Fig. 2e, Tables 1 and S1†).[48] The functional and structural characterization of some of these peptides, pinpointed the key role of TCR–peptide–MHC binding geometry and demonstrated how the chemistry of the peptide can modulate the TCR signaling by perturbing the extracellular receptor-ligand architecture. With the aim of elucidating the molecular basis of non-agonistic high affinity TCR–peptide–MHC interactions occurring *in vivo*, Sibener *et al.* applied yeast display to evolve peptide agonists of a formerly non-signaling TCR thus uncoupling binding affinities from signalling.[49] Selections using yeast display identified stimulatory 9-amino acid peptide ligands for the signaling-refractive TCR that differed by as little as a methylene group (Tables 1 and S1†).[49] With the aim of elucidating the molecular basis of TCR cross-reactivity, Adams *et al.* applied random peptide libraries tethered to a newly circularly permuted MHC-I scaffold displayed on yeast to identify cross-reactive peptides with a wide range of affinities (K_d = 0.1–48 μM) and limited homology to the cognate antigen (Tables 1 and S1†).[50] Similarly, Birnbaum *et al.* combined affinity-based TCR selection of highly diverse yeast-displayed peptide–MHC libraries with deep sequencing to characterize the binding affinity and specificity of hundreds of unique peptide sequences against five different TCRs.[52] Gee *et al.* coupled a single cell TCR analysis method with a refined version of the yeast display library screening approach to discover novel TCR–peptide–MHC specificities in human colorectal adenocarcinoma, thus enabling the identification of novel tumor antigens for

orphan TCRs expressed on tumor-infiltrating lymphocytes (TILs).[53] To better understand the relationship between TCR–peptide–MHC affinity and cross-reactivity in both low and high-affinity regimes, Gee *et al.* engineered an additional weak interaction site, termed "velcro", independent of the canonical interface between the TCR and peptide–MHC. The velcro peptide was identified by screening an 8-amino acid peptide library fused to the amino terminus of the MHC-bound peptide displayed on the surface of yeast (Fig. 2f and g).[54] The addition of the velcro sequence resulted

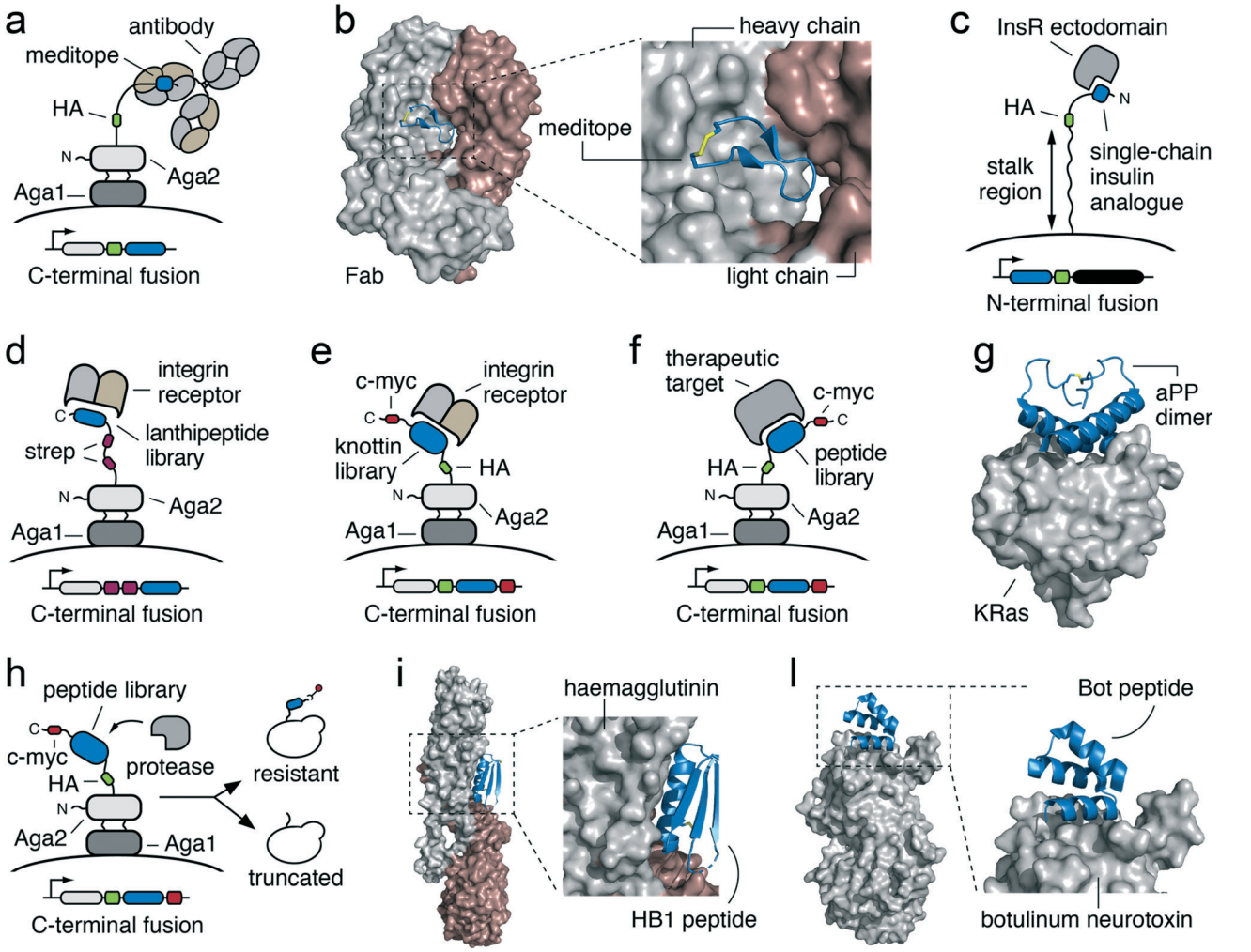

Fig. 3 Schematic representation of cyclic peptides and peptides with a well-defined tertiary structure evolved using yeast display technology. a) The cyclic peptide "meditope" (*blue*) is displayed on the surface of yeast as a C-terminus fusion of the Aga2 protein (*light gray*) and recognized by a specific pocket located in the antigen-binding fragment (Fab) of the therapeutic antibody cetuximab. The light and heavy chains of the antibody are shown in *brown* and *medium gray*, respectively; b) *Left*, crystal structure of the Fab (*brown* and *medium gray surface*) in complex with meditope (*blue cartoon*, PDB code: 4GW1). *Right*, close-up of the Fab pocket occupied by the cyclic peptide meditope. The disulfide bridge of the peptide is shown in *yellow*, the antibody light and heavy chains are colored in *brown* and *medium gray*, respectively; c) the single-chain insulin analogue (*blue*) is displayed on the surface of yeast as a N-terminus fusion of a long and flexible stalk region (*black line*) anchored to the yeast cell wall. Properly folded single-chain insulin analogues retain the ability to bind the ectodomain of the insulin receptor (InsR, *medium gray*); the lanthipeptides (d) and the knottins (e) are displayed on the surface of yeast as a C-terminus of Aga2 subunit (*light gray*) and recognized by a heterodimeric integrin receptor (*brown* and *medium gray*); f) similar approach has been used to display numerous peptides with well-defined tertiary structures (*blue*) on the surface of yeast and detect their binding to multiple therapeutic targets (*medium gray*); g) crystal structure of a dimeric peptide derived from the avian pancreatic polypeptide (aPP, *blue cartoon*) in complex with a KRas mutant (*gray surface*, PDB code: 5WPL). The intermolecular disulfide bond is shown in *yellow*; h) designed peptides with well-defined tertiary structures (*blue*) are displayed on the surface of yeast as a C-terminus fusion of the Aga2 protein (*light gray*) and incubated with a protease. Proteolytic cleavage of the peptides ("truncated" forms) leads to loss of the c-myc tag at the C-terminus and consequent loss of fluorescence. Only yeast cells displaying stable structured peptides ("resistant" forms) retain fluorescence after proteolysis; i) *Left*, crystal structure of a designed peptide with a well-defined tertiary structure (*blue cartoon*) in complex with the hemagglutinin (HA, *brown* and *medium gray*) of influenza A virus PR8 (PDB code: 5VLI). *Right*, close-up of the peptide–HA complex; l) *Left*, crystal structure of a designed peptide with a well-defined tertiary structure (*blue cartoon*) in complex with the botulinum BoNT H_CB neurotoxin (*brown* and *medium gray*, PDB code: 5VID). *Right*, close-up of the complex. The epitope tags flaking the engineered peptides are colored in *green* (HA), *red* (c-myc) and *purple* (strep).

in a 5 to 10-fold increase of the cognate TCR–peptide–MHC affinity thus enabling the characterization of very weak affinity TCR ligands ($K_d > 100$ μM) otherwise difficult to measure (Tables 1 and S1†).[54]

The use of the yeast display has not been limited to the solely purpose of identifying peptide binders with tuned affinity and specificity, but it has also been used to select novel enzyme substrates. Ting and co-workers applied yeast display to isolate kinetically efficient peptide substrates of the *Escherichia coli* lipoic acid ligase (LplA), an ATP-dependent cofactor enzyme that catalyzes the covalent ligation of lipoic acid onto a specific lysine side chain presents on a peptide acceptor (Fig. 2h). Careful library design, an optimized selection scheme, four rounds of *in vitro* directed evolution followed by additional rational mutagenesis allowed the identification of a new 13-amino acid peptide substrate of LplA, named "LplA acceptor peptide 2" (LAP2),[55] that showed a catalytic efficiency (k_{cat}/k_m) for lipoic acid ligation of 0.99 μM^{-1} min^{-1}, >70-fold better than a previously rational designed 22-amino acid peptide named LAP1 that had a $k_{cat}/k_m < 0.0135$ μM^{-1} min^{-1} (Tables 1 and S1†).[56]

3.2. Cyclic peptides

Genetically encoded cyclic peptides are usually generated starting from linear peptides containing two or more cysteine residues in close spatial proximity that undergo oxidation to form disulfide bonds. In contrast to linear analogues, cyclic peptides often show limited conformational flexibility and smaller entropic penalty upon binding to the target thus resulting in molecules with higher affinity and selectivity.[57] Importantly, cyclic peptides with constrained conformations usually exhibit higher stability and resistance to proteolytic degradation.[57]

Van Rosmalen *et al.* combined yeast display and deep mutational scanning to enhance the affinity of "meditope", a phage display derived 12-amino acids disulfide-constrained cyclic peptide that binds a specific pocket located in the antigen-binding fragment (Fab) of the therapeutic antibody cetuximab (Fig. 3a and b).[58] Affinity maturation experiments using double amino acids substitution libraries yielded a pentamutant peptide with 9-fold increase in affinity over the parental one (Tables 2 and S2†).[58] Meditope with superior affinity could be used as a specific non-covalent and paratope-independent tag for targeted drug delivery, molecular imaging and therapeutic drug monitoring.

G-protein-coupled receptors (GPCRs) constitute a large family of proteins that mediate the majority of cellular responses to external stimuli, including numerous cyclic peptides.[59] Somatostatin, also known as somatotropin-release inhibitory factor, is a cyclic peptide that exerts potent inhibitory actions on hormone secretion and neuronal excitability by binding multiple GPCR somatostatin receptors (SSTR1–5).[60] Kondo and colleagues used the 14-amino acid bioactive isoform of somatostatin (S-14, Fig. S1†) and its specific human SSTR5 receptor as model to validate the ability of a novel yeast surface display system to selectively track cyclic peptides with agonistic activity for GPCRs.[61] The technology was named "Cell Wall Trapping of Autocrine Peptide" (CWTrAP) and relies on an engineered yeast strain able to express the green fluorescent protein (GFP) upon GPCR stimulation with an agonistic S-14 peptide fused to an anchoring protein. This new system paves the way for the identification of novel leads with agonistic activity for GPCRs using combinatorial peptide libraries displayed on yeast.

Recently, Chou and colleagues applied a similar strategy to display a single-chain insulin-like peptide on the surface of yeast.[62] The presence of numerous disulfide bonds represents a significant challenge for the correct folding of insulin making its engineering very difficult by many *in vitro* display technologies (Fig. S1†). There is therefore great interest in developing combinatorial tools for the evolution of insulin variants for studying its signaling pathway and to generate novel therapeutics to treat metabolic diseases.[63] Toward this aim, Jeong *et al.* took advantage of a recently described long and flexible stalk to anchor a single-chain insulin analogue to the yeast cell wall (Fig. 3c).[19] Data revealed that the displayed insulin was correctly folded and maintained its ability to bind the insulin receptor (InsR). The methodology was further validated using other single-chain insulin analogues with various

Table 2 Cyclic peptides evolved using yeast display technology. Indicated dissociation constant (K_d), inhibition constant (K_i) and half maximal inhibitory concentration (IC_{50}) values were reported as published. Legend: cetuximab = chimeric (mouse/human) monoclonal antibody targeting EGFR; $\alpha_v\beta_x$ = integrin receptor family; Md1 = Meditope; EETI-II = *Ecballium elaterium* trypsin inhibitor II; AgRP = human agouti-related protein; SOTI = *Spinacia oleracea* trypsin inhibitor; MCoTI = *Momordica cochinchinensis* trypsin inhibitor; CTLA-4 = cytotoxic T lymphocyte-associated antigen 4; n.a. = not available; a = monospecific clones; b = bispecific clones

		Yeast display engineering		
Peptide	Target	Before	After	Ref.
Md1	Cetuximab	K_d = 134.6 nM	K_d = 15.8 nM (~9-fold)	58
Lacticin 481	$\alpha_v\beta_3$	$K_i > 900$ nM	K_i = 2.5–15 nM (>60-fold)	66
EETI-II	$\alpha_v\beta_3$, $\alpha_v\beta_5$	n.a.	IC_{50} = 10–30 nM	68
	$\alpha_v\beta_3$, $\alpha_v\beta_5$	n.a.	IC_{50} = 7 nM[b]	69
	$\alpha_{iib}\beta_3$, $\alpha_v\beta_1$		IC_{50} = 300–500 nM[b]	
AgRP	$\alpha_v\beta_3$	n.a.	K_d = 0.8–15 nM[a]	70
	$\alpha_{iib}\beta_3$		$K_d > 100$ nM[a]	
	$\alpha_v\beta_1$, $_{\alpha v}\beta_5$		$K_d > 500$ nM[a]	
	$\alpha_{iib}\beta_3$	n.a.	K_d = 42–70 nM[b]	71
	$\alpha_v\beta_3$		K_d = 20–30 nM[b]	
	$\alpha_v\beta_1$, $\alpha_v\beta_5$		$K_d > 1000$ nM[b]	
	$\alpha_{iib}\beta_3$		K_d = 60–90 nM[a]	
	$\alpha_v\beta_3$, $\alpha_v\beta_1$, $\alpha_v\beta_5$		$K_d > 1000$ nM[a]	
MCoTI-II	Trypsin	K_i = 2.40 nM	K_i = 19.2–35.8 nM	73
	Matriptase-1	K_i = 80.7 nM	K_i = 0.83–7.8 nM (>10-fold)	
SOTI-III	Trypsin	K_i = 60.6 nM	$K_i > 1000$ nM	
	Matriptase-1	$K_i > 1000$ nM	K_i = 28.9 nM (>34-fold)	
MCoTI-II	CTLA-4	n.a.	K_d = 3.7 μM	75

lengths and confirmed their functionalities. The technique has the potential to be used to construct insulin-like peptide libraries and evolve novel chemical probes or therapeutic molecules.

Lanthipeptides are ribosomally synthesized and post-translationally modified peptides (RiPPs) that display a wide variety of biological activities, from antimicrobial to anti-allodynic. Lanthipeptides are polycyclic peptides characterized by the presence of the thioether-cross-linked amino acids that are critical not only for the activity of the molecule but also for its stability against proteolysis and heat denaturation.[64,65] Given their exquisite properties, there is a lot of interest in applying engineering tools towards the development of novel lanthipeptide analogues with enhanced pharmacological properties and therapeutic utility. By displaying a library of lanthipeptides on the surface of yeast (Fig. 3d), Van der Donk and colleagues were able to identify fully modified peptides with new binding activities against heterodimeric ($\alpha\beta$) integrin receptors, a large family of cell adhesion molecules that are essential for the regulation of cell growth and function.[66] Deep sequencing of FACS sorted libraries containing 6-random positions in the C-ring of class II lanthipeptide lacticin 481 allowed identification of peptides that were enriched over 1000-fold for binding toward the $\alpha_v\beta_3$ integrin. The isolated peptides showed low nanomolar potencies (K_i = 2.5–15 nM) whereas no inhibition was observed for the parent compound (Tables 2 and S2†).[66] This study represents the first example of heterologous expression of bacterial RiPPs in yeast and paves the way for the combinatorial evolution of lanthipeptide variants with new biological activities.

Another example of polycyclic peptides that have been effectively engineered by yeast surface display are the cysteine knots, also called knottins (Fig. S1†).[67] These peptides range in size from 30 to 50 amino acids and are characterized by a core of antiparallel β-strands stabilized by at least three disulfide bonds. The resulting highly constrained and rigid structure endows these peptides with remarkable chemical, thermal and proteolytic stability. Because of their favorable properties, knottins have generated significant interest as diagnostics, therapeutics and research tools.[67] The ability of yeast cells to catalyze efficient disulfide isomerization suits perfectly to knottin peptides containing multiple constraining cysteines. While the eukaryotic machinery of yeast can guarantee correct cysteine pairing patterns, disulfide scrambling can occur using other *in vitro* display techniques. Over the last ten years, Cochran and colleagues have applied yeast surface to successfully engineer several knottins with novel binding properties (Fig. 3e).[68–72] In a pioneering study, Kimura *et al.* applied yeast surface display technology to evolve a 28-amino acid knottin peptide to bind with high affinity the $\alpha_v\beta_3$ integrin receptor.[68] Toward this goal, the authors replaced the 6-amino acid-binding loop of the naturally occurring *Ecballium elaterium* trypsin inhibitor II (EETI-II, Fig. S1†) with a loop of 11-amino acids containing a Arg-Gly-Asp (RGD) motif surrounded by random residues. Surprisingly, although the library screens were performed only against $\alpha_v\beta_3$ integrin, the engineered knottins showed very different integrin specificities. In addition to block the $\alpha_v\beta_3$ integrin, the engineered peptides bound with high affinity also to $\alpha_v\beta_5$ and $\alpha_5\beta_1$ integrins expressed on the surface of glioblastoma cells (Tables 2 and S2†).[68] In a further study Kimura *et al.* used yeast surface display to engineer an EETI-II mutant containing two separate RGD integrin-binding motifs located into different loops.[69] The evolved bispecific knottin bound with high affinities to $\alpha_v\beta_3$ and $\alpha_v\beta_5$ integrins and with low affinity to the related $\alpha_5\beta_1$ and $\alpha_{iib}\beta_3$. In addition, the engineered peptide inhibited tumor cell adhesion to vitronectin, an extracellular matrix protein that binds to $\alpha_v\beta_3$ and $\alpha_v\beta_5$ integrins (Tables 2 and S2†).[69] Similarly, Silverman *et al.* evolved the 34-amino acids C-terminal cysteine-knot peptide of the human neuropeptide agouti-related protein (AgRP, Fig. S1†), to bind the $\alpha_v\beta_3$ integrin with high binding affinity and specificity.[70] Yeast surface display of a library of AgRP in which a 6-amino acid loop was replaced by a 9-amino acid loop of randomized residues flanking the RGD sequence, enabled the engineering of knottin peptides capable of binding cells expressing $\alpha_v\beta_3$ integrins with affinities ranging from 0.8 to 15 nM (Tables 2 and S2†).[70] Furthermore, the engineered peptides were shown to bind specifically to $\alpha_v\beta_3$ integrins and had only minimal or no binding to $\alpha_v\beta_1$, $\alpha_v\beta_5$ and $\alpha_{iib}\beta_3$ integrins expressed on glioblastoma and leukemia cells.[70] In a further study, Silverman *et al.* applied yeast display AgRP-derived libraries to engineer peptides with selective binding only to $\alpha_{iib}\beta_3$ or to both $\alpha_{iib}\beta_3$ and $\alpha_v\beta_3$ integrins with low nanomolar affinities (Tables 2 and S2†).[71]

Additionally, Kolmar and colleagues demonstrated that cysteine-knot peptides MCoTI-II (Fig. S1†) and SOTI-III, two trypsin inhibitors derived from *Momordica cochinchinensis* and *Spinacia oleracea* families, respectively, can also be engineered by using yeast display to block matriptase-1, a type II transmembrane serine protease with possible clinical relevance in cancer and arthritic therapy.[73] Five inhibitor variants, four of the MCoTI-II family and one of the SOTI-III family, were identified and characterized. Enzyme assays revealed inhibition constants in the low nanomolar range for all candidates (Tables 2 and S2†).[73] One sub-nanomolar MCoTI-II-derived binder (K_i = 0.83 nM) with a 43-fold higher selectivity for matriptase-1 was identified. No inhibition was observed when this peptide binder was tested against other related proteases (>12 000-fold selectivity).[73] Similarly, Maaß *et al.* engineered MCoTI-II library capable of binding the cytotoxic T lymphocyte-associated antigen 4 (CTLA-4), an inhibitory receptor expressed by T lymphocytes, that has emerged as a target for immunotherapy of cancer and other diseases.[74] Binding analysis of a yeast display selected clone in its monomeric form revealed an affinity of 3.7 μM (Tables 2 and S2†).[75] Engineered knottins are increasingly been used as molecular imaging agents, therapeutics and drug delivery vehicles.[67] Because of their compact and stable structures, knottins are often refereed as miniproteins that are the topic of our next section.

3.3. Peptides with defined tertiary structure

Though peptides are typically unstructured, many examples of peptides shorter than 50 amino acids that present a well-defined tertiary structure consisting of two or more secondary elements, sequestered hydrophobic cores, and cooperative folds, have been described. These peptides are often referred as miniproteins and they are being increasing investigated for both basic and applied research.[76] While for the majority of genetically encoded peptides the high stability is achieved through cyclization and post-translation modifications, in the case of peptides with a well-defined tertiary structure the stability depends exclusively by its sequence-to-structure relationship and can also occurs without disulfides.[76] Although many small protein scaffolds successfully engineered by yeast surface display have often been denoted as miniproteins,[15] this review will focus exclusively on those that are shorter than 50 amino acids and therefore more easily referable to peptides.

An example of peptide with a well-defined tertiary structure that has been successfully engineered by yeast display is the 45-residue truncated T7 phage gene 2 protein (Gp2). This peptide was identified by Hackel and colleagues thorough a systematic evaluation of known protein topologies existing in the Protein Data Bank (PDB).[77] Gp2 contains an α-helix opposite to a β-sheet with two adjacent solvent-exposed loops amenable to mutation. Its initial size (67 amino acids) was further minimized to generate a smaller variant of 45-amino acid long (Fig. S1†). Using yeast surface display and affinity maturation, Kruziki *et al.* identified target-specific Gp2 molecules with high affinity (K_d = 0.2–18 nM) to four model proteins, including the epidermal growth factor receptor (EGFR), a clinically validated biomarker for imaging and therapy in multiple cancer types (Tables 3 and S3†). All of the identified mutants comprised high thermal stability (T_m = 65–80 °C), which, in some cases, even exceeded the melting temperatures obtained for the wild-type molecule.[77] The highly specific EGFR-targeting Gp2 variant was further effectively used by Kruziki *et al.* as a molecular probe for positron emission tomography (PET) imaging experiments in xenograft mouse model.[78] Recently Chan *et al.* applied yeast display Gp2 libraries with the goal of creating novel InsR inhibitors and diagnostics.[79] The selected Gp2 variants exhibited low nanomolar affinities (K_d = 2.4–13 nM) and specific binding to the receptor (Table 3). Interestingly, all the identified variants contained two cysteine residues in their sequence, otherwise naturally absent in the wild-type sequence (Table S3†).[79] When tested *in vitro*, Gp2 variants inhibited insulin-stimulated monolayer proliferation in both endocrine-sensitive and resistant breast cancer cell lines.[79]

Another peptide with a well-defined tertiary structure that has been lately evolved using yeast display is the 32-amino acid avian pancreatic polypeptide (aPP).[80] The structure of aPP is composed of an N-terminal type II polyproline helix that folds upon a C-terminal α-helix to generate a stable, well-packed hydrophobic core (Fig. S1†). Verdine and colleagues applied yeast surface display to isolate aPP variants with extraordinary high affinity for the effector domain of Ras, a GTPase protein that plays a prominent role in cell proliferation and survival.[81] Mutated over-activated Ras proteins are found in more than 33% of all neoplasms across a broad range of tumor types, and are associated with disease aggressiveness and poor response to treatment. By screening a yeast display library of aPP containing 8 randomized positions on the outward face of the α-helix, McGee *et al.* identified a variant able to bind Ras mutants with nanomolar affinities (K_d = 31–47 nM) and at least ~100-fold specificity over other GTPases containing similar effector domains.[81] Importantly, the engineered peptide directly antagonizes Ras-effector interactions that are essential for the signaling in the cell. Further biophysical experiments revealed that the binder acted as a dimer covalently stabilized by a disulfide bond between cysteine residues present in two separated peptides (Fig. 3f and g). This heterodimeric molecule was further engineered to enhance the nucleotide state selectivity resulting in a variant with sub-nanomolar affinity to all the Ras isoforms and mutants yet preserving selectivity for Ras proteins over other GTPases (K_d > 100 μM; Tables 3 and S3†).[81]

Recently, Rocklin *et al.* combined computational design, next-generation gene synthesis and yeast surface display to assess the folding and stability of >10^4 *de novo* designed peptides with a well-defined tertiary structure.[82] Yeast cell displaying libraries of *de novo* designed peptides, point mutants and control sequences were incubated with varying concentrations of proteases and the stable variants identified using FACS and deep sequencing (Fig. 3h). More than 2500 stable designed peptides were identified. Structural analysis of 4 variants (Fig. S1†) combined to saturation mutagenesis data on 13 designed peptides, indicated that the large

Table 3 Peptides with a well-defined tertiary structure evolved using yeast display technology. Indicated specific target-binding dissociation constants (K_d) were reported as published. Legend: Gp2 = T7 phage gene 2 protein; EGFR = epidermal growth factor receptor; IgG = immunoglobulin G; InsR = insulin receptor; aPP = avian pancreatic polypeptide; KRas = Kirsten rat sarcoma 2 viral oncogene homolog; NRas = Neuroblastoma Ras viral oncogene homolog; HRas = Harvey rat sarcoma viral oncogene homolog; Rap1a = Ras-related protein Rap-1A; RalA = Ras like proto-oncogene A; Rab25 = Ras-related protein Rab-25; BoNT/B = botulinum neurotoxin B; H1 HA = influenza A H1 haemagglutinin; n.a. = not available; m = monomer; d = dimer

		Yeast display engineering		
Peptide	Target	Before	After	Ref.
Gp2	Human EGFR	n.a.	K_d = 7–18 nM	77
	Rat EGFR		K_d = 29 nM	
	Lysozyme		K_d = 0.9 nM	
	Rabbit IgG		K_d = 2.3 nM	
	Goat IgG		K_d = 0.2 nM	
	InsR	n.a.	K_d = 2.4–13 nM	79
aPP	KRas, NRas, HRas	n.a.	K_d = 31–47 nM^m; 0.06–0.18 nM^d	81
	Rap1a		K_d = 4 μM^m; >100 μM^d	
	RalA, Rab25		K_d > 10 μM^m; >100 μM^d	
Bot	BoNT/H_cB	n.a.	K_d = 0.5–13 nM	83
HB1	H1 HA	n.a.	K_d = 2–6 nM	

majority of the molecules were more stable ($T_m > 80$ °C) than any comparably sized monomeric folded peptide found in nature, making them useful tool for a wide range of applications in bioengineering and synthetic biology.[82] Similarly, Chevalier *et al.* integrated computational design and yeast display technology to screen tens of thousands of well-defined tertiary structure peptide binders against two relevant therapeutic targets: influenza A H1 haemagglutinin (HA, Fig. 3i) and botulinum neurotoxin B (BoNT/B, Fig. 3l).[83] All the identified binders were 37 to 43 amino acids long, had melting temperatures greater than 70 °C and exhibited binding affinities ranging from 1 to 20 nM (Tables 3 and S3†). The best of the HA and BoNT/B designs strongly neutralized influenza viruses in culture and protected rat cortical neurons against the entry of the botulinum toxin, respectively. Further *in vivo* studies demonstrated a prophylactic and therapeutic protection with a potency rivalling or surpassing that of antibodies. Lastly, sequential administration of the peptides elicited little or no antibody response demonstrating the low immunogenicity of *de novo* designed molecules.[83] The low immunogenicity combined to a small size, a very high stability, affinity and specificity offer peptides with a well-defined tertiary structure the potentials to become therapeutic and diagnostic agents.

4. Conclusions

While initially developed for the engineering of complex eukaryotic proteins that are difficult to manipulate using other *in vitro* methodologies, yeast display technology is now proving also very useful for the evolution of a wide range of peptide formats. Recent advances in computational design, gene synthesis and deep sequencing, as well as easy access to flow cytometry instruments, have dramatically contributed to the growing success of yeast display over other-directed evolution tools. While some limitations (such as small size library diversities and avidity issues) have been mitigated by the efficient yeast folding machinery and quantitative high-throughput FACS screening, numerous other drawbacks are still restraining the full potentialities of this technique. Differently from other *in vitro* display technologies, the chemical diversity of the genetically encoded peptides displayed on the surface of yeast is still limited to the 20 canonical amino acids.[84] The presence of side chains with similar reactivity limit the possibility of introducing targeted post-translational chemical modifications that could further tune the properties of the displayed peptides and greatly increase their chemical diversity. For example, the diversity of the displayed peptides could potentially be expanded by introducing new chemical entities such as fluorophores, pharmacophores and other biological active groups. Toward this direction, innovative studies describing the display of post-translationally modified peptides[66] and the successful incorporation of non-natural amino acids with orthogonal reactivity on polypeptides displayed on yeast have recently been reported.[85,86] Moreover, the modification of peptides with non-reducible chemical linkers could enhance their rigidity leading to higher stability and binding affinity. In the future, the development and combination of both post-translational and co-translational modifications may provide access to genetically encoded peptides displayed on yeast with greater functional diversity and superior properties for multiple biomedical and biotechnological applications.

Conflicts of interest

There are no conflicts to declare.

Acknowledgements

We thank Dr. Giulia Pasqual and Dr. Laura Cendron for the critical reading of this review.

References

1 S. Koutsopoulos, *Peptide applications in biomedicine, biotechnology and bioengineering*, Woodhead Publishing, 2018.
2 R. D. Süssmuth and A. Mainz, *Angew. Chem., Int. Ed.*, 2017, **56**, 3770–3821.
3 A. D. Cunningham, N. Qvit and D. Mochly-Rosen, *Curr. Opin. Struct. Biol.*, 2017, **44**, 59–66.
4 M. S. Packer and D. R. Liu, *Nat. Rev. Genet.*, 2015, **16**, 379–394.
5 P. A. G. Tizei, E. Csibra, L. Torres and V. B. Pinheiro, *Biochem. Soc. Trans.*, 2016, **44**, 1165–1175.
6 G. P. Smith, *Science*, 1985, **228**, 1315–1317.
7 R. W. Roberts and J. W. Szostak, *Proc. Natl. Acad. Sci. U. S. A.*, 1997, **94**, 12297–12302.
8 J. Hanes and A. Plückthun, *Proc. Natl. Acad. Sci. U. S. A.*, 1997, **94**, 4937–4942.
9 J. A. Francisco, R. Campbell, B. L. Iverson and G. Georgiou, *Proc. Natl. Acad. Sci. U. S. A.*, 1993, **90**, 10444–10448.
10 E. T. Boder and K. D. Wittrup, *Nat. Biotechnol.*, 1997, **15**, 553–557.
11 C. G. Ullman, L. Frigotto and R. N. Cooley, *Briefings Funct. Genomics*, 2011, **10**, 125–134.
12 A. Wada, *Front. Immunol.*, 2013, **4**, 224.
13 A. Galán, L. Comor, A. Horvatić, J. Kuleš, N. Guillemin, V. Mrljak and M. Bhide, *Mol. BioSyst.*, 2016, **12**, 2342–2358.
14 A. Angelini, T. F. Chen, S. de Picciotto, N. J. Yang, A. Tzeng, M. S. Santos, J. A. Van Deventer, M. W. Traxlmayr and K. D. Wittrup, *Methods Mol. Biol.*, 2015, **1319**, 3–36.
15 D. Könning and H. Kolmar, *Microb. Cell Fact.*, 2018, **17**, 32.
16 G. M. Cherf and J. R. Cochran, *Methods Mol. Biol.*, 2015, **1319**, 155–175.
17 C. Andreu and M. L. Del Olmo, *Appl. Microbiol. Biotechnol.*, 2018, **102**, 2543–2561.
18 S. Lim, J. E. Glasgow, M. F. Interrante, E. M. Storm and J. R. Cochran, *Biotechnol. J.*, 2017, **12**, 1–17.
19 C. Mcmahon, A. S. Baier, R. Pascolutti, M. Wegrecki, S. Zheng, J. X. Ong, S. C. Erlandson, D. Hilger, S. G. F.

Rasmussen, A. M. Ring, A. Manglik and A. C. Kruse, *Nat. Struct. Mol. Biol.*, 2018, **25**, 289–296.
20 J. A. Rakestraw, D. Aird, P. M. Aha, B. M. Baynes and D. Lipovsek, *Protein Eng., Des. Sel.*, 2011, **24**, 525–530.
21 M. M. Schmidt, S. A. Townson, A. J. Andreucci, B. M. King, E. B. Schirmer, A. J. Murillo, C. Dombrowski, A. W. Tisdale, P. A. Lowden, A. L. Masci, J. T. Kovalchin, D. V. Erbe, K. D. Wittrup, E. S. Furfine and T. M. Barnes, *Structure*, 2013, **21**, 1966–1978.
22 J. A. Van Deventer, R. L. Kelly, S. Rajan, K. D. Wittrup and S. S. Sidhu, *Protein Eng., Des. Sel.*, 2015, **28**, 317–325.
23 C. A. Cruz-Teran, K. Tiruthani, A. Mischler and B. M. Rao, *ACS Synth. Biol.*, 2017, **6**, 2096–2107.
24 J. J. VanAntwerp and K. D. Wittrup, *Biotechnol. Prog.*, 2000, **16**, 31–37.
25 M. Mammen, S.-K. Choi and G. M. Whitesides, *Angew. Chem., Int. Ed.*, 1998, **37**, 2754–2794.
26 N. London, B. Raveh and O. Schueler-furman, *Curr. Opin. Chem. Biol.*, 2013, **17**, 952–959.
27 S. N. Robertson and R. D. Spring, *Molecules*, 2018, **23**, 1–18.
28 J. Kale, E. J. Osterlund and D. W. Andrews, *Cell Death Differ.*, 2018, **25**, 65–80.
29 T. Moldoveanu, A. V. Follis, R. W. Kriwacki and D. R. Green, *Trends Biochem. Sci.*, 2014, **39**, 101–111.
30 J. T. Opferman, *FEBS J.*, 2016, **283**, 2661–2675.
31 S. Dutta, S. Gullá, T. S. Chen, E. Fire, R. A. Grant and A. E. Keating, *J. Mol. Biol.*, 2010, **398**, 747–762.
32 S. Dutta, T. S. Chen and A. E. Keating, *ACS Chem. Biol.*, 2013, **8**, 778–788.
33 G. W. Foight, J. A. Ryan, S. V. Gulla, A. Letai and A. E. Keating, *ACS Chem. Biol.*, 2014, **9**, 1962–1968.
34 S. Dutta, J. Ryan, T. S. Chen, C. Kougentakis, A. Letai and A. E. Keating, *J. Mol. Biol.*, 2015, **427**, 1241–1253.
35 L. L. Reich, S. Dutta and A. E. Keating, *J. Mol. Biol.*, 2015, **427**, 2135–2150.
36 L. L. Reich, S. Dutta and A. E. Keating, *Methods Mol. Biol.*, 2016, **1414**, 233–247.
37 J. M. Jenson, J. A. Ryan, R. A. Grant, A. Letai and A. E. Keating, *eLife*, 2017, **6**, 1–23.
38 J. M. Jenson, V. Xue, L. Stretz, L. L. Reich and A. E. Keating, *Proc. Natl. Acad. Sci. U. S. A.*, 2018, **115**, 10342–10351.
39 L. D. Walensky, A. L. Kung, I. Escher, T. J. Malia, S. Barbuto, R. D. Wright, G. Wagner, G. L. Verdine and S. J. Korsmeyer, *Science*, 2004, **305**, 1466–1471.
40 R. R. Araghi and A. E. Keating, *Curr. Opin. Struct. Biol.*, 2016, **39**, 27–38.
41 R. R. Araghi, G. H. Bird, J. A. Ryan, J. M. Jenson, M. Godes, J. R. Pritz, R. A. Grant, A. Letai, L. D. Walensky and A. E. Keating, *Proc. Natl. Acad. Sci. U. S. A.*, 2018, **115**, 886–895.
42 J. Neefjes, M. L. M. Jongsma, P. Paul and O. Bakke, *Nat. Rev. Immunol.*, 2011, **11**, 823–836.
43 M. Wieczorek, E. T. Abualrous, J. Sticht, M. Álvaro-Benito, S. Stolzenberg, F. Noé and C. Freund, *Front. Immunol.*, 2017, **8**, 1–16.
44 J. S. Bridgeman, A. K. Sewell, J. J. Miles, D. A. Price and D. K. Cole, *Immunology*, 2012, **135**, 9–18.
45 E. T. Boder, J. R. Bill, A. W. Nields, P. C. Marrack and W. K. John, *Biotechnol. Bioeng.*, 2005, **92**, 485–491.
46 W. Jiang and E. T. Boder, *Proc. Natl. Acad. Sci. U. S. A.*, 2010, **107**, 13258–13263.
47 F. Wen, O. Esteban and H. Zhao, *J. Immunol. Methods*, 2008, **336**, 37–44.
48 J. J. Adams, S. Narayanan, B. Liu, M. E. Birnbaum, A. C. Kruse, N. A. Bowerman, W. Chen, A. M. Levin, J. M. Connolly, C. Zhu, D. M. Kranz and K. C. Garcia, *Immunity*, 2011, **35**, 681–693.
49 L. V. Sibener, R. A. Fernandes, E. M. Kolawole, C. B. Carbone, F. Liu, D. McAffee, M. E. Birnbaum, X. Yang, L. F. Su, W. Yu, S. Dong, M. H. Gee, K. M. Jude, M. M. Davis, J. T. Groves, W. A. Goddard, J. R. Heath, B. D. Evavold, R. D. Vale and K. C. Garcia, *Cell*, 2018, **174**, 672–687.e27.
50 J. J. Adams, S. Narayanan, M. E. Birnbaum, S. S. Sidhu, S. J. Blevins, M. H. Gee, L. V. Sibener, B. M. Baker, D. M. Kranz and K. C. Garcia, *Nat. Immunol.*, 2016, **17**, 87–94.
51 T. P. Riley, L. M. Hellman, M. H. Gee, J. L. Mendoza, J. A. Alonso, K. C. Foley, M. I. Nishimura, C. W. Vander Kooi, K. C. Garcia and B. M. Baker, *Nat. Chem. Biol.*, 2018, **14**, 934–942.
52 M. E. Birnbaum, J. L. Mendoza, D. K. Sethi, S. Dong, J. Glanville, J. Dobbins, E. Özkan, M. M. Davis, K. W. Wucherpfennig and K. C. Garcia, *Cell*, 2014, **157**, 1073–1087.
53 M. H. Gee, A. Han, S. M. Lofgren, J. F. Beausang, J. L. Mendoza, M. E. Birnbaum, M. T. Bethune, S. Fischer, X. Yang, R. Gomez-Eerland, D. B. Bingham, L. V. Sibener, R. A. Fernandes, A. Velasco, D. Baltimore, T. N. Schumacher, P. Khatri, S. R. Quake, M. M. Davis and K. C. Garcia, *Cell*, 2018, **172**, 549–563.e16.
54 M. H. Gee, L. V. Sibener, M. E. Birnbaum, K. M. Jude, X. Yang, R. A. Fernandes, J. L. Mendoza, C. R. Glassman and K. C. Garcia, *Proc. Natl. Acad. Sci. U. S. A.*, 2018, **115**, 7369–7378.
55 S. Puthenveetil, D. S. Liu, K. A. White, S. Thompson and A. Y. Ting, *J. Am. Chem. Soc.*, 2009, **45**, 16430–16438.
56 M. Fernández-suárez, H. Baruah, L. Martínez-hernández, K. T. Xie, J. M. Baskin, C. R. Bertozzi and A. Y. Ting, *Nat. Biotechnol.*, 2007, **25**, 1483–1487.
57 R. Derda and M. R. Jafari, *Protein Pept. Lett.*, 2018, **25**, 1–25.
58 M. Van Rosmalen, B. M. G. Janssen, N. M. Hendrikse, A. J. Van Der Linden, P. A. Pieters, D. Wanders, T. F. A. De Greef and M. Merkx, *J. Biol. Chem.*, 2017, **292**, 1477–1489.
59 W. I. Weis and B. K. Kobilka, *Annu. Rev. Biochem.*, 2018, **87**, 897–919.
60 T. Günther, G. Tulipano, P. Dournaud, C. Bousquet, Z. Csaba, H.-J. Kreienkamp, A. Lupp, M. Korbonits, J. P. Castaño, H.-J. Wester, M. Culler, S. Melmed and S. Schulz, *Pharmacol. Rev.*, 2018, **70**, 763–835.
61 J. Ishii, N. Yoshimoto, K. Tatematsu, S. Kuroda, C. Ogino, H. Fukuda and A. Kondo, *PLoS One*, 2012, **7**, 1–10.
62 M. Jeong, J. Rutter and D. H. Chou, *Biochemistry*, 2019, **58**, 182–188.
63 A. N. Zaykov, J. P. Mayer and R. D. DiMarchi, *Nat. Rev. Drug Discovery*, 2016, **15**, 425–439.

64 P. J. Knerr and W. A. van der Donk, *Annu. Rev. Biochem.*, 2012, **81**, 479–505.
65 L. M. Repka, J. R. Chekan, S. K. Nair and W. A. van der Donk, *Chem. Rev.*, 2017, **117**, 5457–5520.
66 K. J. Hetrick, M. C. Walker and W. A. Van Der Donk, *ACS Cent. Sci.*, 2018, **4**, 458–467.
67 J. R. Kintzing and J. R. Cochran, *Curr. Opin. Chem. Biol.*, 2016, **34**, 143–150.
68 R. H. Kimura, A. M. Levin, F. V. Cochran and J. R. Cochran, *Proteins: Struct., Funct., Bioinf.*, 2009, **77**, 359–369.
69 R. H. Kimura, D. S. Jones, L. Jiang, Z. Miao, Z. Cheng and J. R. Cochran, *PLoS One*, 2011, **6**, e16112.
70 A. P. Silverman, A. M. Levin, J. L. Lahti and J. R. Cochran, *J. Mol. Biol.*, 2009, **385**, 1064–1075.
71 A. P. Silverman, M. S. Kariolis and J. R. Cochran, *J. Mol. Recognit.*, 2011, **24**, 127–135.
72 S. J. Moore, C. L. Leung, H. K. Norton and J. R. Cochran, *PLoS One*, 2013, **8**, e60498.
73 B. Glotzbach, M. Reinwarth, N. Weber, S. Fabritz, M. Tomaszowski, H. Fittler, A. Christmann, O. Avrutina and H. Kolmar, *PLoS One*, 2013, **8**, e76956.
74 B. Rowshanravan, N. Halliday and D. M. Sansom, *Blood*, 2018, **131**, 58–67.
75 F. Maaß, J. Wüstehube-lausch, S. Dickgießer, B. Valldorf, M. Reinwarth, H. Schmoldt, M. Daneschdar, O. Avrutina and H. Kolmar, *J. Pept. Sci.*, 2015, **21**, 651–660.
76 E. G. Baker, G. J. Bartlett, K. L. Porter Goff and D. N. Woolfson, *Acc. Chem. Res.*, 2017, **50**, 2085–2092.
77 M. A. Kruziki, S. Bhatnagar, D. R. Woldring, V. T. Duong and B. J. Hackel, *Chem. Biol.*, 2015, **22**, 946–956.
78 M. A. Kruziki, B. A. Case, J. Y. Chan, E. J. Zudock, D. R. Woldring, D. Yee and B. J. Hackel, *Mol. Pharmaceutics*, 2016, **13**, 3747–3755.
79 J. Y. Chan, B. J. Hackel and D. Yee, *Mol. Cancer Ther.*, 2017, **16**, 1324–1335.
80 A. M. Hodges and A. Schepartz, *J. Am. Chem. Soc.*, 2007, **129**, 11024–11025.
81 X. J. H. Mcgee, S. Y. Shim, S. Lee, P. K. Swanson, S. Y. Jiang, M. A. Durney and G. L. Verdine, *J. Biol. Chem.*, 2018, **293**, 3265–3280.
82 G. J. Rocklin, T. M. Chidyausiku, I. Goreshnik, A. Ford, S. Houliston, A. Lemak, L. Carter, R. Ravichandran, V. K. Mulligan, A. Chevalier, C. H. Arrowsmith and D. Baker, *Science*, 2017, **357**, 168–175.
83 A. Chevalier, D. A. Silva, G. J. Rocklin, D. R. Hicks, R. Vergara, P. Murapa, S. M. Bernard, L. Zhang, K. H. Lam, G. Yao, C. D. Bahl, S. I. Miyashita, I. Goreshnik, J. T. Fuller, M. T. Koday, C. M. Jenkins, T. Colvin, L. Carter, A. Bohn, C. M. Bryan, D. A. Fernández-Velasco, L. Stewart, M. Dong, X. Huang, R. Jin, I. A. Wilson, D. H. Fuller and D. Baker, *Nature*, 2017, **550**, 74–79.
84 C. Heinis and G. Winter, *Curr. Opin. Chem. Biol.*, 2015, **26**, 89–98.
85 J. A. Van Deventer, D. N. Le, J. Zhao, H. P. Kehoe and R. L. Kelly, *Protein Eng., Des. Sel.*, 2016, **29**, 485–494.
86 J. T. Stieglitz, H. P. Kehoe, M. Lei and J. A. Van Deventer, *ACS Synth. Biol.*, 2018, **7**, 2256–2269.

